

Condensation and Growth of Kirkendall Voids in Intermetallic Compounds

Kerstin Weinberg and Thomas Böhme

Abstract—A model for the simulation of Kirkendall voiding in metallic materials is presented based on vacancy diffusion, elastic-plastic and rate-dependent deformation of the material. Starting with a phenomenological explanation of the Kirkendall effect we briefly discuss the consequences on the reliability of microelectronic components. Then, a constitutive model for void nucleation and growth is introduced, which can be used to predict the temporal development of voids in solder joints during thermal cycling. We present numerical studies and discuss the potential of the results for the failure analysis of joining connections.

Index Terms—Intermetallic compounds, Kirkendall effect, plastic deformation, vacancy diffusion, void distribution, void growth, void nucleation.

I. INTRODUCTION

MICROELECTRONIC circuit units consist of the functional chip unit itself and its packaging, which includes several electromechanical connections, e.g., solder joints between different metal layers. Failure of these metallic components is a well established cause of failure of the whole microelectronic system. The general setup of a typical microelectronic system is illustrated in Fig. 1 exemplarily for the flip chip packaging. Solder balls as well as small, nowadays, lead-free joints which are typically made of Sn-containing alloys (e.g., Sn–Ag or Sn–Ag–Cu) hold the multilayered unit in position. In addition, the solder joints provide electrical conductivity between the coppered layers. “Aging” of the solder alloy, such as phase separation, coarsening, or the formation of intermetallic compounds (IMCs), as well as the formation and growth of pores and cracks in the vicinity of heterogeneities significantly effect the life expectation of the joints and considerably influence the reliability of the whole component.

During manufacturing, the (molten) Sn-rich solder wets the copper pad, and IMCs are formed due to an interfacial reaction [9]. In particular, the copper-rich Cu_3Sn is expected to grow adjacent to the copper substrate, and Cu_6Sn_5 will form adjacent to the Sn-based solder, cf., Fig. 2. However, in prac-

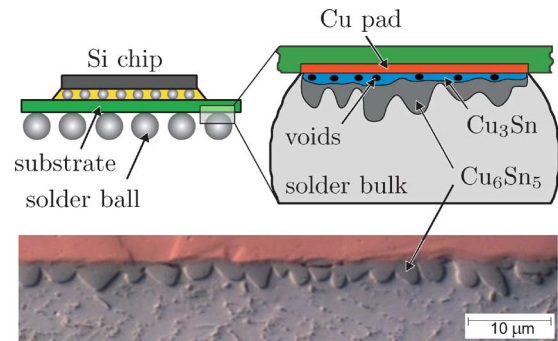


Fig. 1. Intermetallic compounds at copper–solder interfaces in microelectronic components. Micrograph courtesy of K. Müller, Neue Materialien Bayreuth, Germany, 2005.

tice both IMCs form together with further intermetallics to irregular-shaped layers of initially 2–5 μm height. Due to the reflow process and to the thermal cycling during service, the solder joint ages and the IMCs grow and may reach a thickness of 20 μm and more, cf., [12], [19]. Another consequence of solder joint aging is the condensation and growth of so-called Kirkendall voids (mainly) within the intermetallic zones. The physics behind this mechanism may be sketched as follows: neighboring phases or compounds change in a way that the volume of one region grows and the volume of the another phase reduces. In our case such regions are the IMCs in which Cu_3Sn compounds grow on the expense of Cu_6Sn_5 by $\text{Cu}_6\text{Sn}_5 \rightarrow 2\text{Cu}_3\text{Sn} + 3\text{Sn}$, and the three free Sn atoms will attract nine Cu atoms to form $\text{Sn} + 3\text{Cu} \rightarrow \text{Cu}_3\text{Sn}$. Moreover, the diffusion of Cu from the pad via the interface $\text{Cu}/\text{Cu}_3\text{Sn}$ into Cu_3Sn is much slower than the diffusion of Cu from Cu_3Sn into the Cu_6Sn_5 scallops, which also cannot be “corrected” by the inverse diffusion of Sn through the $\text{Cu}_6\text{Sn}_5/\text{Cu}_3$ interface. As a consequence of this unbalanced diffusion, vacancies are left which condense to form Kirkendall voids, cf., Fig. 2. Additional vacancies and defects in the crystal lattices are generated by plastic deformation of the solder material and assist in the process of void growth and material degradation.

The scope of this paper is to model the condensation and growth of such voids in IMCs within a continuum mechanical framework. To this end, we idealize the material as a homogeneous medium with arbitrarily distributed vacancies and study the formation of voids and their growth up to significant size. In the following section, we outline the constitutive equations which enables us to model the void condensation and growth process. Subsequently, we study short-term and long-term effects and present exemplary results. Finally, the temporal development of an ensemble of differently sized voids is investigated by means of a void size distribution function.

Manuscript received June 15, 2008. This work is based on joint activities of the authors at the Institute of Mechanics (TU Berlin) and was supported by the German Federal Environmental Foundation (DBU). This work is based on joint activities of the authors at the Institute of Mechanics (TU Berlin) and was recommended for publication by Associate Editor K. Jonnalagadda upon evaluation of the reviewers comments.

K. Weinberg is with Lehrstuhl für Festkörpermechanik, Institut für Mechanik und Regelungstechnik, Universität Siegen, 57068 Siegen, Germany (e-mail: kerstin.weinberg@tu-berlin.de; weinberg@imr.mb.uni-siegen.de).

T. Böhme is with ThyssenKrupp Steel AG, Division Auto, Werkstoffkompetenzzentrum, 47166 Duisburg, Germany.

Color versions of one or more of the figures in this paper are available online at <http://ieeexplore.ieee.org>.

Digital Object Identifier 10.1109/TCAPT.2008.2010057

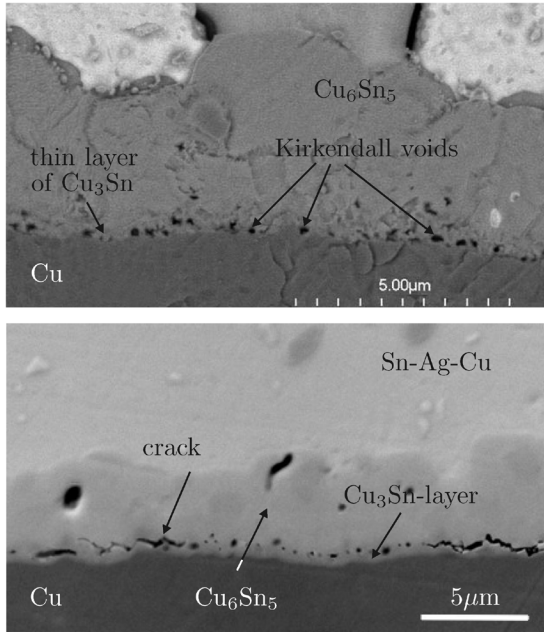


Fig. 2. First row: Kirkendall voids within the Cu_3Sn layer; photograph from [11]. Second row: Crack initiation by void coalescence after 1000 thermal cycles between $-40\text{ }^\circ\text{C}$ and $125\text{ }^\circ\text{C}$; photograph from [19].

II. VOID NUCLEATION BY VACANCY DIFFUSION

To explore the feasibility of void condensation out of the scale of crystal lattice defects as a void-nucleating mechanism, we employ here a model of *vacancy condensation*. To this end, let us consider a small void possibly just a few atomic spacings in diameter surrounded by a supersaturated background vacancy concentration c_b generated, e.g., by unbalanced diffusion in the sense of Kirkendall. To render the problem analytically tractable, we idealize the defect to be spherical with characteristic radius a , the diffusion constants to be isotropic, and we assume that a steady-state vacancy concentration profile is maintained all times, i.e., $\partial c_{\text{vac}}/\partial t \ll \partial J_{\text{vac}}/\partial x$, where J_{vac} is the vacancy flux. This eliminates the time dependence of the solution and confers spherical symmetry to the problem. With b being the (large) radius of the basin of attraction around the void, cf., Fig. 3, and $b/a \rightarrow \infty$, the diffusion equation for *volume concentration* c reduces to the following boundary value problem in spherical coordinates:

$$\frac{\partial}{\partial r} \left(r^2 \frac{\partial c}{\partial r} \right) = 0 \quad (1)$$

subject to the boundary conditions

$$c(r=b) = c_b, \quad c(r=a) = c_a = c_0 e^{d/a}. \quad (2)$$

Here, the equilibrium vacancy concentration near a free surface is given by

$$c_0 = e^{-E_v/kT} \quad (3)$$

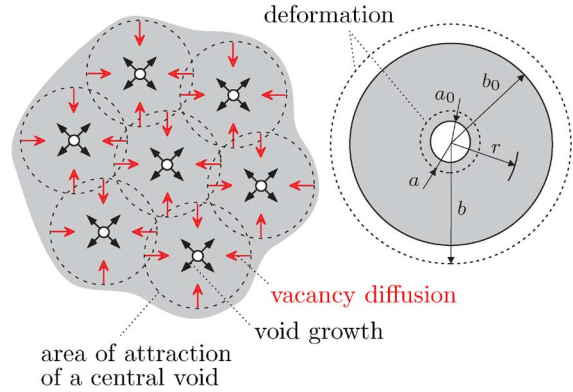


Fig. 3. Model of vacancy diffusion and model of a single void before and after deformation.

and the concentration c_a at the void surface follows as above with $d = 2\gamma V_V/kT$ due to the Gibbs–Thomson effect. In these expressions, γ is the surface tension, V_V the atomic volume, k the Boltzmann constant, and E_v is the free-energy gain/loss resulting from adding a vacancy into the system. The solution of (1) and (2) is elementary, namely

$$c(r) = c_b - (c_b - c_a) \frac{a}{r}. \quad (4)$$

For void growth to take place, there must be a net flux of vacancies *into* the void, which requires $c_b > c_a$. This in turn requires

$$c_b > c_0 \exp\left(\frac{2\gamma V_V}{a_0 kT}\right). \quad (5)$$

For very small values of a_0 or c_b this inequality is not satisfied and voids fail to grow. However, the value of radius a_0 which equals relation (5) at a given value of c_b marks the inception of void growth, i.e., a *critical nucleation size*. Furthermore, the flux density J is defined to be the change of volume per unit area and time, *viz.*

$$J(r=a) = -\frac{1}{4\pi a^2} \frac{d}{dt} \left(\frac{4}{3} \pi a^3 \right) = -\dot{a}(r). \quad (6)$$

Applying additionally Fick's law $J(r) = -D_V(\partial c/\partial r)$ to (6) yields for voids of radius a by means of (4)

$$\dot{a}(a) = \frac{D_V}{a} (c_b - c_0 e^{d/a}) \quad (7)$$

where D_V is the vacancy diffusion coefficient. As the void grows, c_a decreases according to (2)₂ which amplifies the concentration gradient towards the void and, thus, accelerates the void growth. The rate of void growth may be computed by means of (7).

Following the strategy of Wagner [16] but allowing for an additional source term $s(t)$ the background vacancy concentration c_b can be subjected to a “void volume balance” of the form

$$\begin{aligned}\dot{c}(t) &= s(t) - \int_{a_{\text{vac}}}^{a_{\text{max}}} \tilde{d}(a, t) \dot{a}(a) 4\pi a^2 da \\ &= s(t) - \int_{a_{\text{vac}}}^{a_{\text{max}}} \tilde{d}(a, t) D_V (c_b - c_0 e^{d/a}) 4\pi a da.\end{aligned}\quad (8)$$

Here, $\tilde{d}(a, t)$ denotes a *void size distribution function* describing the fraction of voids with a specific size $a \in [a_{\text{vac}}, a_{\text{max}}]$ at time t . At this point, we neglect the statistics and consider only one void size $\tilde{d}(a, t) = 1$, but we will study different void distributions in Section VI. The source term $s(t)$ in (8) represents a *vacancy production rate* due to unbalanced diffusion which is caused, e.g., by the different diffusion coefficients of the migrating substances. Please note that (7) has been derived in [5] in a thermodynamic consistent manner (for a constant number of vacancies). In particular, the vacancy diffusion coefficient D_V has been identified as the tracer diffusion coefficient of vacancies.

In addition, we ask for an energetic formulation of the above vacancy diffusion problem. In particular, we look for a *diffusion rate potential* $\Phi(\dot{a}, a)$, for which the variational form

$$\frac{\delta \Phi(\dot{a}, a)}{\delta \dot{a}} = 0 \quad (9)$$

holds. For that reason, we follow the strategy in [4] and multiply (7) with a characteristic factor E_v/D_V . A subsequent integration w.r.t. \dot{a} finally results in

$$\Phi(\dot{a}, a) = \frac{E_v \dot{a}^2}{2D_V} - \frac{E_v \dot{a}}{a} (c_b - c_0 e^{d/a}). \quad (10)$$

III. CONSTITUTIVE MODEL OF VOID GROWTH

Once voids are nucleated, diffusion is not the only mechanism which triggers their growth within the IMCs. To set up a general *variational model* for void growth in a deforming material, we postulate the existence of a free energy density function associated with the deformation of expanding voids and embedding material. Additionally we require the time-dependent constitutive equations to derive from power potentials. Thence, we assume the power of the external forces acting on the material to be *completely* compensated by the change of its free energy and its rate potentials.

Let us now ask, which energy contributions result from the deformation of *one* void subjected to 1) the power P of a remote pressure $p(t)$. These are: 2) the energy of the free void surface S , 3) the deformation energy W of the embedding material, and 4) the rate power of creep deformation Ψ and diffusion Φ . Additional energy and power contributions may play a role in specific regimes, e.g., the kinetic energy in case of a very

rapid loading, cf., [18]. Now an action integral $\mathcal{I}(\dot{a})$ can be formulated as sum of all rate of energy and power contributions. Hamilton’s principle simply requires stationarity of the action integral $\delta \mathcal{I}(\dot{a}) = 0$, or, equivalently

$$\frac{\delta}{\delta \dot{a}} \left[\frac{d}{dt} (W + S) + \Psi + \Phi - P \right] = 0. \quad (11)$$

In what follows, we imagine the material to be a conglomerate of (initially very small) spherical voids each at every instance completely embedded in the material, i.e., we exclude here the process of coalescence, cf., Fig. 3. Consider now a void surrounded by a sphere of influence of material with radius b and let it expand for some reason. Presuming a *volume preserving deformation* it holds for all $r \in [a, b]$

$$\frac{d}{dt} \frac{4\pi}{3} (r^3 - a^3) = 0 \Rightarrow b = (b_0^3 - a_0^3 + a^3)^{\frac{1}{3}} \quad (12)$$

in which the index 0 refers to the initial state, cf., Fig. 3. The kinematic relation (12) will be employed subsequently to express functions of radius b as functions of current void radius a and the initial geometry. Furthermore, the rate of straining of the void surrounding material can be defined as

$$\dot{\epsilon} \stackrel{(\text{def})}{=} \frac{\partial \dot{r}}{\partial r} = \frac{\partial}{\partial r} \left(\frac{a^2 \dot{a}}{r^2} \right) = \frac{2a^2}{r^3} \dot{a} \quad (13)$$

where r is the radius of void surrounding material; see Fig. 3.

In what follows we consider the different energy contributions 1)–4) in detail.

A. External Power

The external power put into the system by an applied (positive or negative) pressure $p(t)$ reads

$$P_{\text{tot}} = \frac{d}{dt} \int_V p(t) dV$$

and for one void we obtain

$$P(\dot{a}, a) = p(t) 4\pi a^2 \dot{a}. \quad (14)$$

In the solder material under consideration here, the effect of thermal cycling on the growth of voids is of particular interest. To this end, temperature cycles $T(t)$ are considered to strain the material and to induce a pressure of the form

$$p(t) = \kappa^*(a) 3\alpha [T_0 - T(t)] \quad (15)$$

where κ^* is the effective bulk modulus and α is the thermal expansion coefficient. Following a classical approach of homogenization, cf., [7] and [10], we obtain for an assemblage of spher-

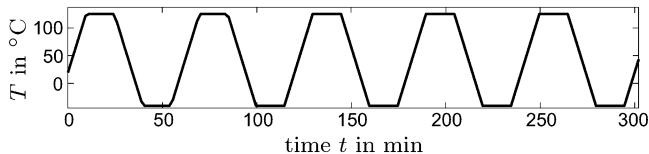


Fig. 4. Thermal cycling between -40 °C and 125 °C, cycles of 60 min with 15-min hold time.

ical voids enclosed in an isotropic material with bulk modulus κ and shear modulus μ the effective bulk modulus κ^* as

$$\kappa^* = \kappa \left(1 - \frac{a^3}{b^3} \frac{3\kappa + 4\mu}{3\kappa + 4\mu b^3/a^3} \right). \quad (16)$$

The temperature $T(t)$, given in (15), cycles between -40 °C and 125 °C within one hour, in which 15 min at up-soak and low-soak temperature, respectively, see Fig. 4.

B. Surface Energy

The surface energy of one void with radius $a(t)$ is written as

$$S(a) = 4\pi a^2 \gamma \quad (17)$$

where γ is the surface energy per unit undeformed area [N/m].

C. Elastic–Plastic Deformation Energy

The deformation energy for the elastic-plastic material response can be derived as follows. We presume a Ramberg–Osgood power law

$$\epsilon = \epsilon^e + \frac{\sigma_0}{E} \left(\frac{\sigma}{\sigma_0} \right)^n \quad (18)$$

where σ and ϵ are the effective stress and strain, respectively. Furthermore, ϵ^e denotes the elastic strain component and $E \equiv E(T)$ and $\sigma_0 \equiv \sigma_0(T)$ represent temperature dependent Young's modulus and initial yield stress. Exponent $n \in [1, \infty)$ determines the stress-strain curve; in particular $n = 1$ prescribes linear elasticity, whereas $n \rightarrow \infty$ enforces perfect (rigid) plasticity. In order to resolve (18), let us assume the elastic strain to be given and decompose $\epsilon = \epsilon^e + \epsilon^p$. Then, the dissipated energy of the deformation per unit volume can be computed from

$$\begin{aligned} \int_0^t \sigma_y \dot{\epsilon}^p d\bar{t} &= \int_0^{\epsilon^p} \sigma_y d\bar{\epsilon}^p \\ &= \frac{n\sigma_0}{n+1} \left(\frac{E}{\sigma_0} \right)^{\frac{1}{n}} (\epsilon - \epsilon^e)^{\frac{n+1}{n}} \end{aligned} \quad (19)$$

and with reference strain $\epsilon_0 = \sigma T/E$ the dissipated deformation energy for one void with surrounding material follows as

$$W(a; T) = \int_a^b \frac{n\sigma_0\epsilon_0}{n+1} \left(\frac{\epsilon - \epsilon^e}{\epsilon_0} \right)^{\frac{n+1}{n}} 4\pi r^2 dr. \quad (20)$$

Let us now refer to the kinematic relation in (13) and assume that the void radius history $a(t)$ grows monotonically from a_0 to a_1 , then decreases monotonically from a_1 to a_2 , and so on. The integration of (13) with respect to the time gives

$$\begin{aligned} \epsilon(r_0, t) &= \frac{2}{3} \log \left(\frac{a_1^3 + r_0^3 - a_0^3}{r_0^3} \right) + \frac{2}{3} \log \left(\frac{a_1^3 + r_0^3 - a_0^3}{a_2^3 + r_0^3 - a_0^3} \right) \\ &\quad + \frac{2}{3} \log \left(\frac{a_3^3 + r_0^3 - a_0^3}{a_2^3 + r_0^3 - a_0^3} \right) + \dots \end{aligned} \quad (21)$$

and grouping terms corresponding to increasing and decreasing intervals yields

$$\epsilon(r_0, t) = \frac{2}{3} \log \left(\frac{q(t)^3 + r_0^3 - a_0^3}{r_0^3} \right) - \frac{2}{3} \log \left(\frac{a^3(t) + r_0^3 - a_0^3}{q^3(t) + r_0^3 - a_0^3} \right) \quad (22)$$

where $q(t)$ is the maximum radius attained by voids of the current size a ,

$$q(t) = \max_{0 \leq \tau \leq t} a(\tau) \quad (23)$$

i.e., $q(t)$ is a monotonically increasing function for every history of $a(t)$. Then, the expression in (22) can be summarized, viz.

$$\epsilon(r_0, t) = \frac{2}{3} \log \left[\frac{(q^3(t) + r_0^3 - a_0^3)^2}{r_0^3 (a^3(t) + r_0^3 - a_0^3)} \right] \quad (24)$$

and with (12) the dissipated deformation energy in a shell surrounding the void is

$$\begin{aligned} W(a, q; T) &= 4\pi \int_{a_0}^{b_0} \frac{n\sigma_0\epsilon_0}{n+1} \\ &\quad \times \left[\frac{2}{3\epsilon_0} \log \left(\frac{(q(t)^3 + r_0^3 - a_0^3)^2}{r_0^3 (a(t)^3 + r_0^3 - a_0^3)} \right) - \frac{\epsilon^e}{\epsilon_0} \right]^{\frac{n+1}{n}} r_0^2 dr. \end{aligned} \quad (25)$$

It is worth mentioning that the function in (25) is trackable by analytical means only in the special case of $n \rightarrow \infty$. Moreover, in moderate hardening materials we know the elastic strain component to be $\epsilon^e \approx \epsilon_0$. Therefore, we set the last term in brackets to one but guarantee the energy to be not negative, i.e., $W \geq 0$.

D. Rate-Dependent Deformation (Creep)

A creep-power potential is formulated in order to capture the effect of the rate of deformation on the rate of straining. Experimental observations reported, e.g., in [1], indicate that the

material near a void is subjected to a state of stress that is likely to cause power-law creep, i.e.,

$$\dot{\epsilon} = \left(\frac{\sigma_y}{\sigma_0} \right)^m \dot{\epsilon}_c \exp(-Q_c/RT) \quad (26)$$

where $\dot{\epsilon}$ is the strain rate, m is a creep exponent, and $\dot{\epsilon}_c$ is a material constant. The temperature dependence of the strain rate is controlled by the thermal activation energy Q_c . Here, we summarize the last terms in (26) to a *reference strain rate*, $\dot{\epsilon}_0 = \dot{\epsilon}_c \exp(-Q_c/RT)$, with small values of $\dot{\epsilon}_0$ corresponding to creep dominated deformation and $\dot{\epsilon}_0 \rightarrow \infty$ to a time independent behavior. The creep–power potential per unit volume is defined by

$$\int_0^{\dot{\epsilon}} \sigma_y d\bar{\epsilon} = \frac{m\sigma_0\dot{\epsilon}}{m+1} \left[\left(\frac{\dot{\epsilon}}{\dot{\epsilon}_0} + 1 \right)^{\frac{m+1}{m}} - 1 \right]. \quad (27)$$

For simplicity we assume now a linear rate dependence, $m = 1$, and by integration over the volume follows the creep potential for one spherical shell as

$$\begin{aligned} \Psi(\dot{a}, a) &= \int_a^b \frac{\sigma_0}{2\dot{\epsilon}_0} \left(\frac{2a^2|\dot{a}|}{r^3} \right)^2 4\pi r^2 dr \\ &= \frac{\sigma_0}{\dot{\epsilon}_0} \int_{a_0}^{b_0} \left(\frac{a^2|\dot{a}|}{a^3 + r_0^3 - a_0^3} \right)^2 8\pi r_0^2 dr_0 \\ &= \frac{2\sigma_0}{\dot{\epsilon}_0} \frac{4\pi a^3}{3} \left| \frac{\dot{a}}{a} \right|^2 \left(1 - \frac{a^3}{a^3 + b_0^3 - a_0^3} \right) \end{aligned} \quad (28)$$

where we again make use of (13).

Setting the external power equal the “sum of the internal powers” according to ansatz (11) yields an *ordinary differential equation* for the void size $a(t)$. In particular, for growing voids and for $n \rightarrow \infty$ in (25) we obtain the expression

$$\begin{aligned} 0 &= -4\pi p(t)a^2 + \frac{8\pi}{3}\sigma_0 a^2 \log \left(\frac{b_0^3 - a_0^3 + a^3}{a^3} \right) \\ &\quad + \frac{16\sigma_0\pi}{3\dot{\epsilon}_0} a^4 \dot{a} \left(\frac{1}{a^3} - \frac{1}{b_0^3} \right) + 8\pi a\gamma \\ &\quad + \frac{E_v \dot{a}}{D_V} - \frac{E_v}{a} (c_b - c_a) \end{aligned} \quad (29)$$

which can be solved (numerically) for all different void sizes of interest. We will outline selected results subsequently.

IV. NUCLEATION OF VOIDS OUT OF SMALL DEFECTS

At first, we study the nucleation of voids, i.e., the formation of pores out of vacancy sized defects. It can easily be seen from (29) that for very small values of a_0 the diffusion term dominates. In the initial stages of void growth, the elastic–plastic material response is of minor influence. As well we neglect the external loading for a start and the equation of motion reads

$$\dot{a} = \frac{D_V}{E_v} \left[8\pi a\gamma - \frac{E_v}{a} (c_b - c_0 e^{d/a}) \right]. \quad (30)$$

TABLE I
MATERIAL CONSTANTS FOR DIFFUSION

D_V [$\frac{m^2}{s}$]	c_0	c_b	d [m]	s [$\frac{1}{s}$]	γ [$\frac{N}{m}$]
10^{-17}	10^{-6}	10^{-4}	$5 \cdot 10^{-6}$	10^{-7}	1

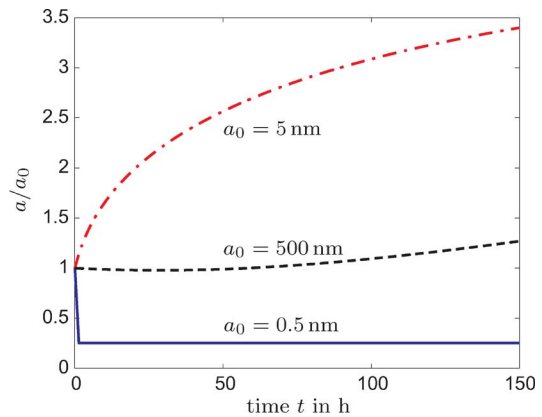


Fig. 5. Condensation and growth of voids with different initial radii a_0 driven by an interplay of diffusion and surface energy contributions.

Thus, the void condensation process is driven by an interplay of vacancy diffusion and surface energy contributions. In particular, for (5) to be satisfied the initial size of the defect must exceed a critical nucleation radius which is here approximately 2–3 times the vacancy size (0.25 nm). To keep voids growing, a vacancy production source is required, otherwise the voids either collapse or reach a steady state—depending on the magnitude of surface tension. In the material under consideration here, the vacancy production results from the unbalanced diffusion, cf. [2]. It is known that copper diffuses interstitially in tin and tin diffuses substitutional in copper and the difference in diffusivity is orders of magnitudes. Therefore, its rate of vacancy production may be assumed to be a function of the diffusion coefficients, i.e., $s(t) = s(t, D_{Cu}, D_{Sn})$. Moreover, an additional source of vacancy production is plastic deformation. However, in this paper we approximate the unknown vacancy production rate by a constant, cf. Table I.

Although Cu–Sn intermetallics are of great interest for the electronic packaging industry, the available material data on such compounds vary considerably, see, e.g., [3], [6], [14] and references therein. With typical values summarized in Table I, we obtain for the solution of (30) the results¹ displayed in Fig. 5. Small defects with an initial radius of $a_0 = 0.5$ nm (twice the size of a vacancy in copper) collapse immediately. Defects of size slightly greater than nucleation size will grow with a rate of void growth depending on the vacancy production rate. On the other hand, big voids, e.g., $a_0 = 500$ nm, basically fail to grow; here, the influence of diffusion is too small for significant void growth.

Fig. 6 shows the same void growth model but now *with* external loading, i.e., the voids are subjected to a pressure history

¹The ODEs of (30) have been solved numerically using the Matlab solver ODE45 as well as an explicit second-order Runge–Kutta procedure.

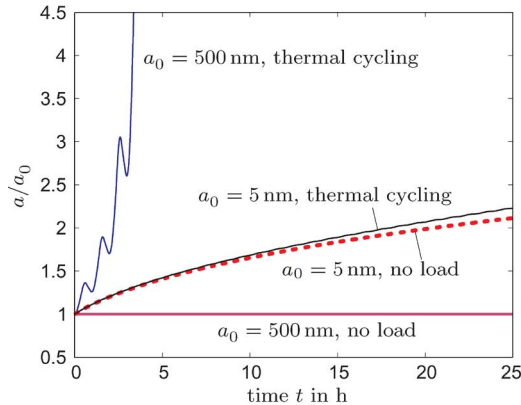


Fig. 6. Influence of the external load induced by subjecting the material to the temperature cycles of Fig. 4 on the diffusion-driven void growth of two voids.

TABLE II
ELASTIC-PLASTIC MATERIAL CONSTANTS²

E [GPa]	κ [GPa]	μ [GPa]	σ_0 [MPa]	α [1/K]
100	80	50	450	$19 \cdot 10^{-6}$

²Experimental data courtesy of Prof. Müller, Institute of Mechanics, TU Berlin, Germany.

induced by thermal cycling. On relatively small voids, this pressure has little effect, their growth is in first instance given by diffusional effects. However, if the void size reaches a significant magnitude the void grows unbounded—a clearly nonphysical effect—which shows the necessity to incorporate elastic-plastic deformation into the model. This effect should be considered in the following section.

V. GROWTH OF VOIDS DUE TO THERMAL CYCLING

The full model of Section III is now studied for medium-sized and big voids with material parameter given in Table II. Note that the elastic-plastic deformation energy contribution in (29) is simplified in order to get an analytical expression; a computation of the full model requires a numerical integration of (25). In Fig. 7, we see the different rates of growth for medium-sized and big voids. Here, we neglect creep effects at first, i.e., $\dot{\epsilon}_0 \rightarrow \infty$.

Both void sizes are subjected to the same thermal cycling of Fig. 4, but their evolution history depends strongly on the initial void size. In particular, smaller voids clearly grow slower than their initially big companions. That supports the experimental observation of several (relatively) large Kirkendall voids in IMCs. The differences in the void size versus time response for the two cases of elastic-plastic material behavior ($n = 5$) and perfect plastic approximation ($n \rightarrow \infty$) are small, the final void size is basically determined by the external loading. Therefore, a simplified approximation as given in (29) seems to be justified. Let us point out that the diffusion effects invoke a “smoothing” of the void growth curves. Even if the underlying elastic-plastic theory is time independent, the material response has no sharp edges as the load history would suggest.

Fig. 8 displays the void size versus time for different reference strain rates. Small values of $\dot{\epsilon}_0$ clearly damp the evolution of voids. However, after enough time has passed the final void size

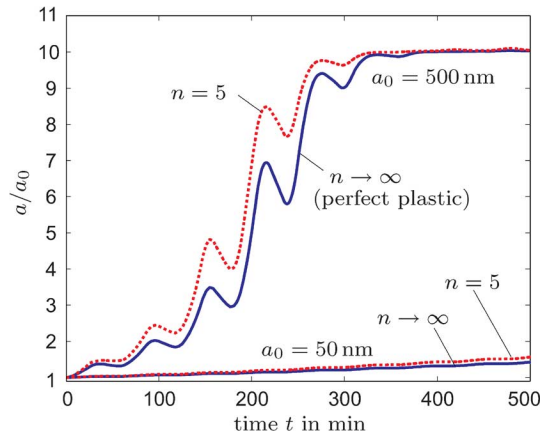


Fig. 7. Growth of a medium-sized and large void induced by thermal cycling for two elastic-plastic material laws according to (18): $n = 5$ and perfect plasticity.

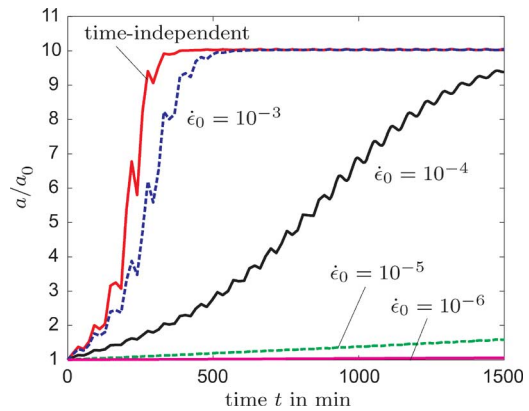


Fig. 8. Effect of creep on the growth of voids of size $a_0 = 500$ nm for different reference strain rates.

will reach the same value as in the time-independent case as can be seen from the curves for $\dot{\epsilon}_0 = 10^{-4}$ and $\dot{\epsilon}_0 = 10^{-3}$ in Fig. 8.

VI. EVOLUTION OF A VOID ENSEMBLE

In order to investigate an *ensemble* of voids with different initial radii we introduce—as already indicated in Section II—a void size distribution function $\tilde{d}(a, x, t)$. To derive an evolution equation for the void distribution we make use of a mesoscopic concept described in detail, e.g., in [13], [17], and [18]. In this paper, we do not account for a dependence of the void distribution on the spatial position x , and set $\tilde{d}(a, x, t) = \tilde{d}(a, t) \equiv \tilde{d}$. Then, we establish for a constant number of voids a balance equation for the void size distribution \tilde{d} in the following form:

$$\frac{\partial \tilde{d}}{\partial t} + \frac{\partial}{\partial x} [\tilde{d}v(x, t)] + \frac{\partial}{\partial a} [\tilde{d}\dot{a}(a)] = 0. \quad (31)$$

The value of $\dot{a}(a)$ can be calculated from the constitutive model introduced in Sections II and III. Moreover, we neglect the spatial velocity of the material element under consideration $v \doteq 0$, so that the second term in (31) vanishes.

To solve (31) numerically, the spatial and temporal derivatives were discretized by *finite differences*. The solution of (29) is obtained by means of a second-order Runge-Kutta method.

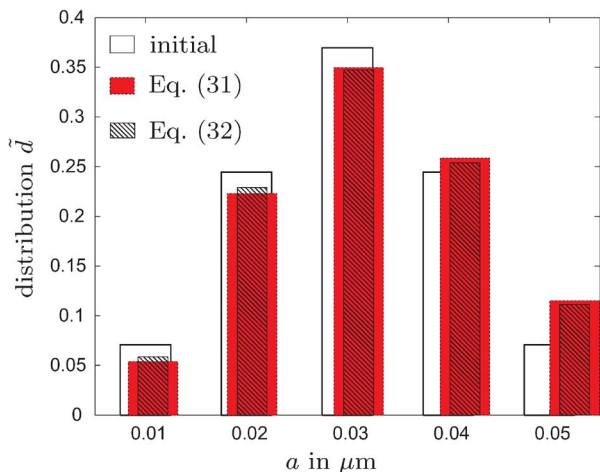


Fig. 9. Comparison of the numerical solution of (31) and (32) for five different radii after two thermal cycles.

For ease of computation we also solved the quasi-linear pendant of (31), *viz.*

$$\frac{\partial \tilde{d}}{\partial t} + \dot{a}(a) \frac{\partial \tilde{d}}{\partial a} = 0. \quad (32)$$

As is shown exemplarily in Fig. 9, both equations yield almost identical results. However, to solve the full (31) a significant finer spatial discretization is required. Therefore, we proceed here with solutions of (32). Furthermore, for a better understanding of the results we neglect any void production, *i.e.*, $s(t) \doteq 0$ in (8). However, there is no extra effort to include the production term into the simulations and in (31) and (32).

We start with a discretized Gaussian distribution of 15 different void radii, $a = 10, \dots, 150$ nm. Within several stages of thermal cycling, we obtain the temporal development of \tilde{d} as illustrated in Fig. 10. The initially symmetric distribution changes to an asymmetrical distribution in such a way that the fraction of smaller voids decreases and the bigger voids grow. Such results are well known from so-called LSW-theories for Ostwald ripening, [16], where bigger “grains” grow at the expense of the smaller ones due to the Gibbs–Thomson effect. In our model, this effect also appears in the first stages of void growth, in which vacancy diffusion dominates. During proceeding growth the voids reach a size, for which the evolution is characterized primarily by elastic–plastic deformation. For such stages, the distribution function considerably differs from a typical LSW distribution. In particular, the number of large voids extremely exceeds the number of small voids.

A different view on the evolution of void size distribution shows Fig. 11. The first plot displays the size distribution of small voids in the beginning of thermal loading. In the long range (second plot in Fig. 11), the growth of the bigger voids driven by elastic–plastic deformation by far exceeds the growth of small voids. The final distribution substantially differs from the initial Gaussian form. In particular, the void regimes primarily consists of large voids, which may allow the assumption of crack formation by void coalescence in the immediate future (*cf.*, Fig. 2).

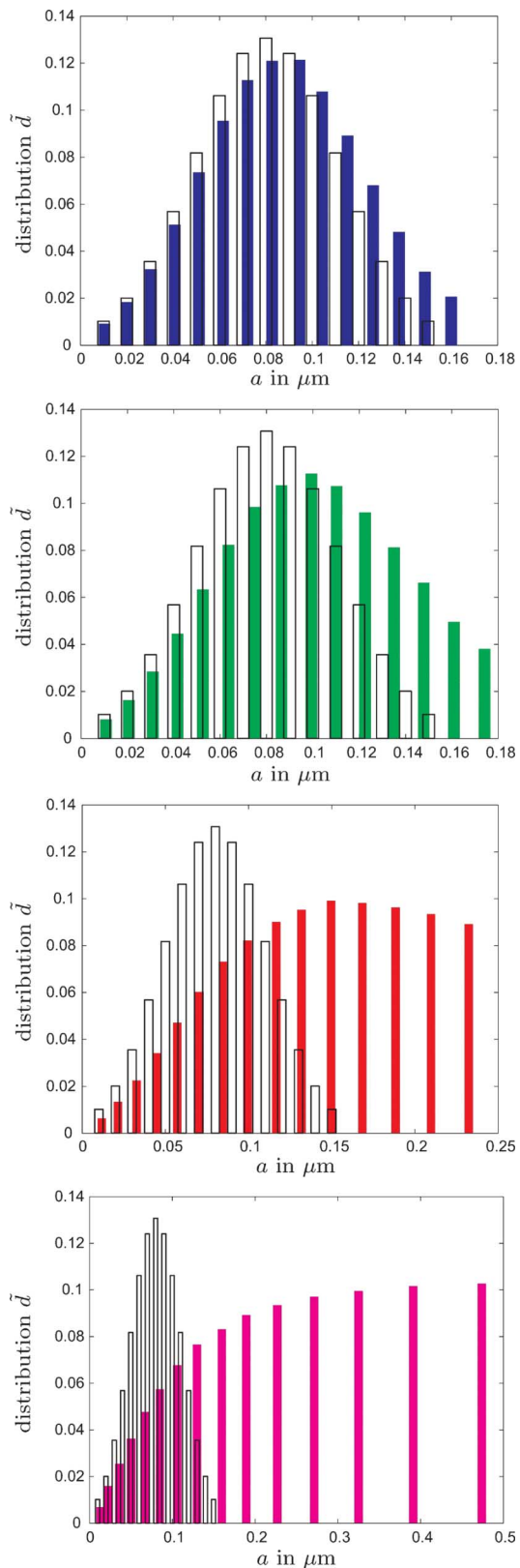


Fig. 10. Development of an initial Gaussian void distribution after 1, 2, 5, and 10 thermal cycles.

Second, we study a distribution of void sizes \tilde{d} , which—in a more realistic manner—accounts for the dominance of small voids in the initial state. To this end, we assume an exponential

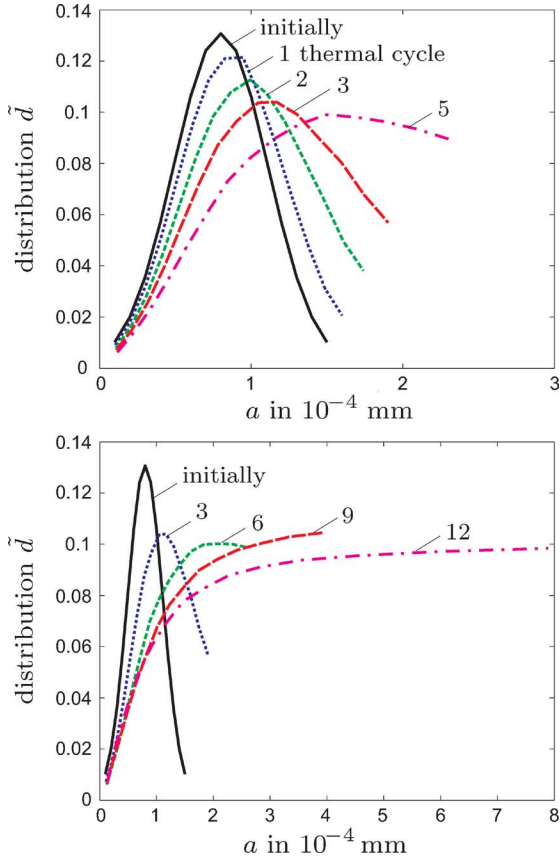


Fig. 11. First row: short time behavior of \tilde{d} . Second row: long time behavior of \tilde{d} .

distribution of 25 voids with $a = 10, \dots, 250$ nm. As displayed in Figs. 12 and 13, we observe again a growth of the fraction of big voids on cost of the smaller ones. In particular, the void size a reaches large values, and the distribution function is stretched over a wide range of void sizes. Here, we stopped the simulations after a void volume fraction of $\approx 2/3$ is reached. Note that our model does not account for void growth due to coalescence. Unfortunately, this limits the predictive capabilities of the void size distribution analysis. However, already a significant amount of large voids in a material clearly indicates the onset of failure.

VII. CONCLUSION

We presented a constitutive model to predict the condensation and growth of Kirkendall voids in elastic–plastic metals, in particular in the IMCs occurring at the interface of microelectronic solder joints. To this end, the influence of vacancy diffusion, surface energy, and elastic–plastic and creep deformation on the evolution of void ensembles during thermal cycling was investigated. It turns out that nano-voids collapse, whereas voids which are small but exceed a critical radius (of a few vacancies) grow driven by diffusional effects. On the other hand, the growth of bigger voids is primarily driven by elastic–plastic deformation of the void surrounding material. We found that work hardening plays a minor role and, as expected, creep decelerates the void growth.

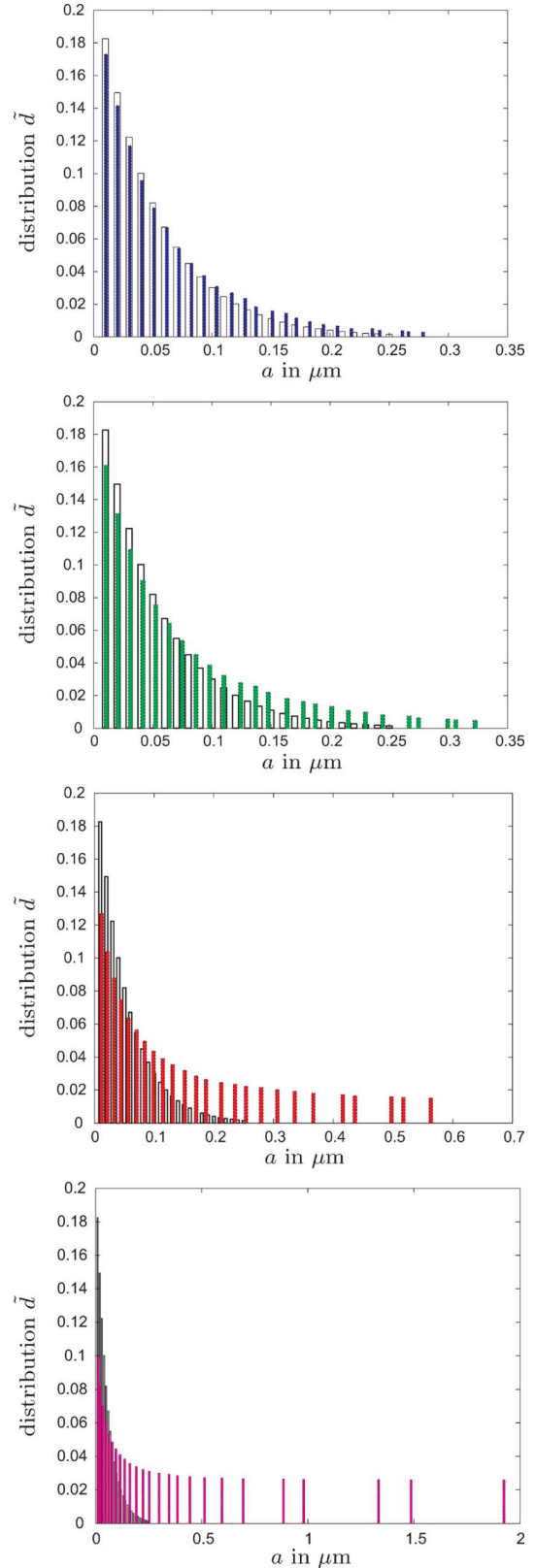


Fig. 12. Development of an initially *exponentially decreasing* void size distribution after 1, 2, 5, and 10 thermal cycles.

Furthermore, we studied the temporal development of void ensembles under thermal cycling. Here, the presented model for

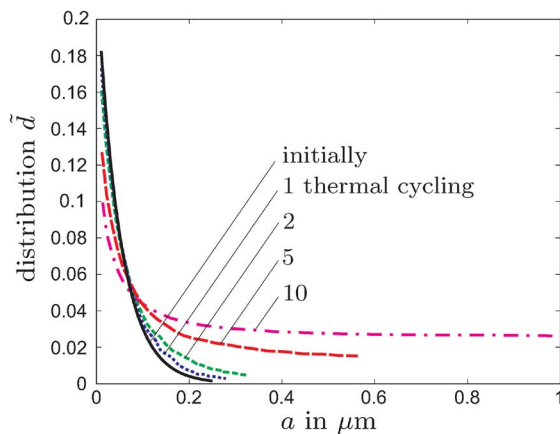


Fig. 13. Compact illustration of the evolution of the distribution function for different numbers of thermal cycles.

void growth is employed to (numerically) solve the balance of the void size distribution function. We found that the evolving distribution initially resembles the ones known from LSW theories, whereas the distribution during proceeded loading evolves such that the amount of large voids drastically increases. Such behavior correlates to experimental studies on Kirkendall voids, cf. [11], [19] and may indicate failure by void growth and coalescence, cf. [8], [15].

The presented results are applicable to derive the temporal evolution of the effective properties of intermetallics. The constitutive model shall be incorporated in finite-element analysis tools on the material point level to study the mechanical behavior of IMCs under realistic loading regimes. Such analyses then allow for a better prediction of live time and strength of microelectronic joining connections.

REFERENCES

- [1] A. F. Bower and L. B. Freund, "Analysis of stress-induced void growth mechanisms in passivated interconnects," *J. Appl. Phys.*, vol. 74, pp. 3855–3868, 1993.
- [2] J. W. Cahn and J. E. Hilliard, "Spinodal decomposition: A reprise," *Acta Metall. Mater.*, vol. 19, pp. 151–161, 1971.
- [3] B. Chao, S. H. Chae, X. Zhang, K. H. Lu, J. Im, and P. S. Ho, "Investigation of diffusion and electromigration parameters for Cu–Sn intermetallic compounds in Pb-free solders using simulated annealing," *Acta Mater.*, vol. 55, no. 8, pp. 2805–2814, 2007.
- [4] A. Cuitino and M. Ortiz, "Ductile fracture by vacancy condensation in FCC single crystals," *Acta Metall. Mater.*, vol. 44, pp. 427–436, 1995.
- [5] F. D. Fischer and J. Svoboda, "Void growth due to vacancy supersaturation—A non-equilibrium thermodynamics study," *Scripta Mater.*, vol. 58, no. 2, pp. 93–95, 2008.
- [6] G. Galyon, "Annotated tin whisker bibliography and anthology," *IEEE Trans. Electron. Packag.*, vol. 28, no. 1, pp. 94–122, Jan. 2005.
- [7] Z. Hashin, "Analysis of composite-materials—A survey," *J. Appl. Mech.-T. ASME*, vol. 50, no. 3, pp. 481–505, 1983.
- [8] J. W. Hutchinson, "Plasticity at the micron scale," *Int. J. Solids Structures*, vol. 37, pp. 225–238, 2000.

- [9] H. K. Kim and K. N. Tu, "Kinetic analysis of the soldering reaction between eutectic SnPb alloy and Cu accompanied by ripening," *Phys. Rev. B*, vol. 53, no. 23, pp. 16027–16034, 1996.
- [10] K. J. Lee and R. A. Westerman, "Elastic properties of hollow-sphere-reinforced composites," *J. Composite Mater.*, vol. 4, pp. 242–252, 1970.
- [11] Z. Mei, M. Ahmad, M. Hu, and G. Ramakrishna, "Kirkendall voids at Cu/solder interface and their effects on solder joint reliability," in *Proc. 55th Electron. Compon. Technol. Conf.*, Orlando, FL, 2005, pp. 415–420.
- [12] R. E. Pratt, E. I. Stromswolda, and D. J. Quesnel, "Effect of solid-state intermetallic growth on the fracture toughness of Cu/63Sn-37Pb solder joints," *IEEE Trans. Compon. Packag. Technol.*, vol. 19, no. 1, pp. 134–141, Mar. 2005.
- [13] C. Papenfuss, P. Ván, and W. Muschik, "Mesoscopic theory of microcracks," *Arch. Mech.*, vol. 55, no. 5–6, pp. 459–477, 2003.
- [14] J. F. Shackelford, *Werkstofftechnologie für Ingenieure*, 6th ed. Munich, Germany: Pearson Studium, 2005.
- [15] V. Tvergaard, "Material failure by void growth to coalescence," *Adv. Appl. Mech.*, vol. 27, pp. 83–151, 1990.
- [16] C. Wagner, "Theorie der Alterung von Niederschlägen durch Umlösen (Ostwald-Reifung)," *Z. Elektrochem.*, vol. 65, no. 7–8, pp. 581–591, 1961.
- [17] K. Weinberg and T. Böhme, "Mesoscopic modeling for continua with pores: Biological soft tissue," *J. Non-Equil. Thermody.*, vol. 33, no. 1, pp. 1–24, 2008.
- [18] K. Weinberg and T. Böhme, "Mesoscopic modeling for continua with pores: Dynamic void growth in visco-plastic metals," *J. Non-Equil. Thermody.*, vol. 33, no. 1, pp. 25–45, 2008.
- [19] L. Xu and J. H. L. Pang, "Interfacial IMC and Kirkendall void on SAC solder joints subject to thermal cycling," in *Proc. 7th Electron. Packag. Technol. Conf.*, Singapore, 2005, vol. 2, pp. 863–867.



Kerstin Weinberg studied mechanical engineering with emphasis on applied mechanics, received the Ph.D. degree about an hp-finite element technique for contact problems from the University of Magdeburg, Magdeburg, Germany, in 1995, and the Venia Legendi degree in mechanics from the Institute for Mechanics, Technical University of Berlin, in 2003.

She is a Full Professor and head of the Chair for Solid State Mechanics, University of Siegen, Siegen, Germany. She has worked in several research groups, for instance in the Numerical Mathematics Group of

Prof. C. Carstensen in Kiel, Germany, or in the Computational Mechanics group of Prof. M. Ortiz at the California Institute of Technology, Pasadena. Her special interests are modeling and simulation of failure mechanism in ductile metals and biological materials, such as soft tissue. Furthermore, she works on material issues in microelectronic devices, e.g., determining of material data of lead-free solder alloys with nanoindentation or failure analysis by large-scale finite-element analysis.



Thomas Böhme studied physical engineering science at the Technical University of Berlin, Berlin, Germany, and received the Ph.D. degree in phase separation and coarsening processes in lead-free solder alloys under Prof. Müller from the Chair of Continuum Mechanics and Materials Theories, Institute of Mechanics, Technical University of Berlin.

He is currently with the Center of Materials Excellence, ThyssenKrupp Steel AG, Duisburg, Germany. His fields of interest are thermodynamics and mechanics of solid materials, in particular modeling/simulation of microstructural phenomena in solders and steels, atomistic models for the determination of materials data, and the description of damage mechanism on the mesoscopic scale.